International Journal of Heat and Mass Transfer 71 (2014) 349–360

Contents lists available at ScienceDirect

International Journal of Heat and Mass Transfer

journal homepage: www.elsevier.com/locate/ijhmt

Two-phase flow dynamics in a micro channel with heterogeneous surfaces

Sung Chan Cho, Yun Wang *

Renewable Energy Resources Lab (RERL), Department of Mechanical and Aerospace Engineering, The University of California, Irvine, Irvine, CA 92697-3975, USA

ARTICLE INFO

Article history:
Received 2 May 2013
Received in revised form 29 October 2013
Accepted 7 December 2013

Keywords:
Two-phase flow
Hydrophobic
Hydrophilic
Rough surface
Visualization
Experiment
Model

ABSTRACT

In this paper, two-phase flows in a micro channel with heterogeneous surfaces are investigated both experimentally and numerically. The heterogeneity in a micro rectangular channel is characterized by three hydrophilic channel walls plus one hydrophobic one; and the hydrophobic surface is either smooth or rough (roughness: 226–550 nm rms for the smooth surface and 21.5–28.9 μm rms for the rough). Results on an entirely hydrophilic smooth channel (roughness ~1.3 nm rms) are also presented for comparison. Two-phase flows are visualized through two different angles: (1) a top view; and (2) a cross-sectional view. It is observed that the surface wetting property and roughness affect the presence site of liquid water flow: liquid water is preferentially present in the two hydrophilic corners when one channel wall is hydrophobic. As a result, two-phase pressure, patterns, and stability differ from the purely hydrophilic channel. Rough surface is found to affect two-phase flow. Model predictions, obtained from both empirical formula based on the Lockhart–Martinelli parameter and two-fluid approach, along with model parameters optimization using experimental data. Real-time pressures are presented to show the effects of channel surface properties on pressure drop.

1. Introduction

Two-phase flows in micro channels are encountered in a wide range of industrial applications. In channels, liquid flow usually stays over wall surface while gas flow stays in the core region of a channel, thus channel surface properties can greatly influence two-phase flow characteristics [1]. In PEM fuel cells, liquid water, originated from water production by the oxygen reduction reaction (ORR) in the cathode, must be removed efficiently by channel gas flow. To avoid liquid coverage over gas diffusion layers (GDL) and ensure effective oxygen transport to the reaction site, GDLs are generally treated hydrophobic, thus liquid flow preferably stays on the other three hydrophilic channel surfaces. In micro channels, surface tension and capillary force are important [2,3]. In addition, physical conditions (e.g., roughness) on the channel surface and channel geometry may impact two-phase flow.

Several studies have been attempted to understand effects of surface properties on two-phase flow. Cubaud et al. [4] experimentally investigated surface modification and its effects on two-phase flow in micro channels. Air–water two-phase flow was tested in 525 μm square channels for both hydrophilic ($9° < \theta < 25°$) and hydrophobic surfaces ($\theta = 120°$). It is stressed out that contact angle is important in determining flow patterns. Choi et al. [5] investigated two-phase flow in rectangular channels with a hydraulic diameter of 490–507 μm and the impact of surface condition on flow pattern and pressure drop. Bubbly, elongated bubble and liquid bridge flow patterns were observed in hydrophilic channels while stratified and stratified with entrainment patterns were observed for the case with hydrophobic surface. They also pointed out flow patterns affect pressure drop. Takamasa et al. [6] evaluated the effect of wall wettability on the flow characteristics in a vertical pipe. The tube of a 20 mm diameter was coated with a thin film (thickness <10 μm) for wettability control. Hydrophilic ($\theta \leqslant 7°$), acrylic ($43° < \theta < 47°$) and hydrophobic ($135° < \theta < 150°$) pipes were tested. Surface properties may alter the boundary of pattern transition. The surface's impact on pressure drop was found to be insignificant in their study. Lee and Lee [7] conducted a similar study in mini channels of a 1.46–2.00 mm diameter. The pattern transition between slug and annulus shifts towards lower gas velocity when using hydrophobic surface. Phan et al. [8] investigated surface wettability and two-phase pressure experimentally. A 0.5×5 mm rectangular channel with surface contact angle of 26°, 49°, 63° and 103°, respectively, was tested; and they found that a higher contact angle leads to a higher pressure drop. Lee and Lee [9] tested three different surface conditions (glass, polyurethane, Teflon) in tubes with a diameter ranging 1.62–2.16 mm. They found that two-phase pressure increases with contact angle. A prediction model was also proposed.

* Corresponding author. Tel.: +1 949 824 6004; fax: +1 949 824 8585.
E-mail address: YUNW@UCI.EDU (Y. Wang).

0017-9310/$ - see front matter © 2013 Elsevier Ltd. All rights reserved.
http://dx.doi.org/10.1016/j.ijheatmasstransfer.2013.12.023

In addition, surface roughness can affect single-phase pressure drop [10]; few works were reported on the effects of surface roughness on two-phase flow. Wu and Cheng [11] indicated that single-phase pressure can be affected by surface roughness even for laminar flow in micro-channels. Olekhnovitach et al. [12] investigated inaccuracy of existing two-phase models that arises from neglecting surface roughness. Cavallini et al. [13] measured two-phase pressure for smooth and rough circular tubes (stainless and copper tubes with mean roughness of 1.3–2.0 μm). Previous correlations underpredict pressure for micro-channels with rough surface. A new correlation was proposed to take into account surface roughness.

Suman and Kumar [14] analytically showed that surface tension is an important factor determining the critical heat input of micro heat pipes. Peterson and Ma [15] also showed impact of contact angle on heat transport capacity. Wong and Lin [16] experimentally studied the effects of evaporator's surface wettability for micro heat pipe. The evaporative resistances under a given heat flux are different among surface contact angles. Qu et al. [17] compared various surface contact angles of a micro heat pipe with triangular cross-section. Both conventional surface (uniform wettability) and functional surface (different wettabilities for evaporator, adiabatic section, and condenser) are tested. They showed the functional surface with contact angle of 10°–30°–45° has the highest liquid flow rate in the adiabatic section. Wu and Cheng [18] experimentally investigated the effects of surface wettability and roughness on the Nusselt number and friction constant for micro heat exchangers. In most cases, a more hydrophilic surface led to a higher Nusselt number and friction constant. A rougher surface yields a higher friction factor and Nusselt number. Hsieh and Lin [19] tested deionized water, methanol, their mixture, and ethanol solution in rectangular micro channels. Hydrophilic and hydrophobic surfaces are prepared using the Ultra Violet (UV) treatment. They showed a higher heat transfer coefficient for hydrophilic surface than that for hydrophobic surface.

Though many studies were attempted to explore the effects of surface properties on two-phase flow characteristics in micro/mini channels, few works investigated two-phase flow in a micro-channel with both hydrophobic and hydrophilic walls. In the first paper of this research series [20], we explore two-phase flow in a hydrophilic micro channel. In this paper, the focus is placed on surface conditions, more specifically, smooth hydrophilic, smooth hydrophobic, and rough hydrophobic walls. Cross-sectional views of two-phase flow are presented, along with pressure measurement and model prediction. A great amount of effort is made on visualization of two-phase pattern and location, which is necessary to reveal two-phase dynamics and explain experimental observation in two-phase pressure measurement.

2. Experimental

2.1. Experimental setup

A rectangular micro channel (dimension: $1.68 \times 1.00 \times 150\ mm^3$), similar to that used in Ref. [20], is prepared for experiment and visualization. Fig. 1 shows schematic of the experiment setup and the test section. To modify channel surface property, a thin layer, either a carbon paper or PTFE sheet, was placed between the base and channel plate. Three surface conditions were chosen

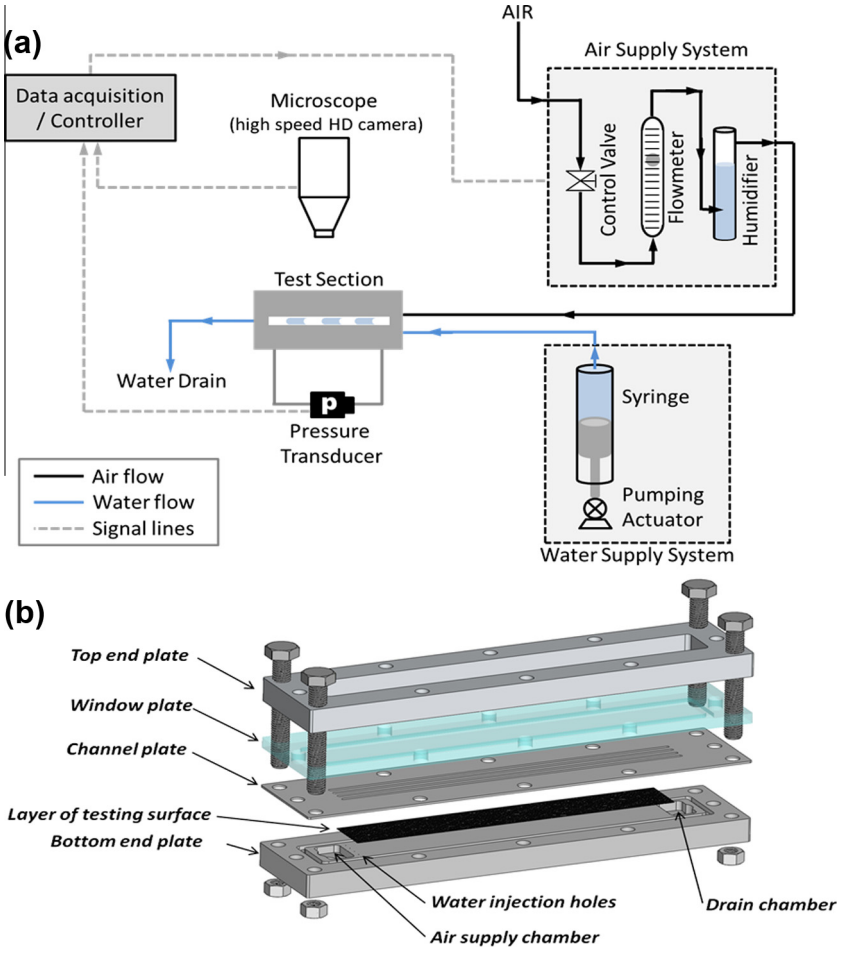

Fig. 1. Schematic of: (a) flow loop of the experiment; (b) the test section for two-phase flow experiment.

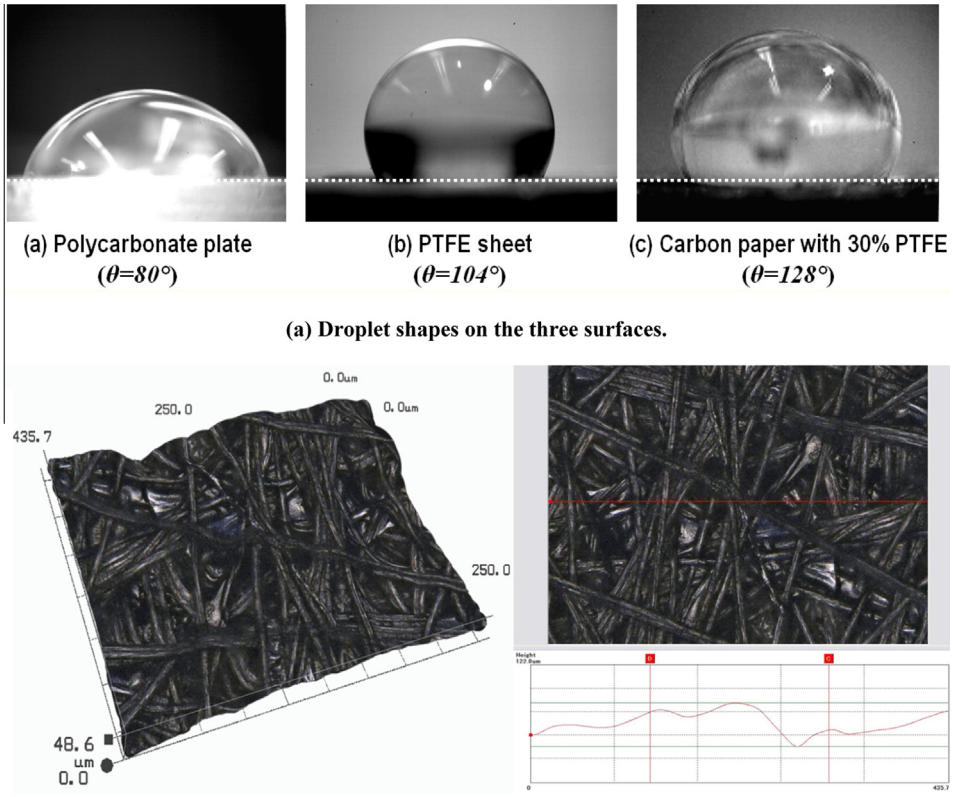

Fig. 2. Droplet shapes on the three surfaces (a); and 3-D image of the rough carbon-paper surface (3-D scan, 700×) (b).

Table 1
Surface properties of the three experimental materials.

Surface material	Contact angle	Roughness	Remarks
Plastic (Polycarbonate) plate	80°	~1.3 nm rms	Smooth/ hydrophilic
PTFE sheet	104°	550–226 nm rms	Smooth/ hydrophobic
Carbon paper	128°	21.5–28.9 μm rms	Rough/ hydrophobic

to investigate the effects of wettability and roughness: (1) smooth, hydrophilic Polycarbonate plate; (2) smooth, hydrophobic PTFE sheet, and (3) rough, hydrophobic carbon paper (Toray TGP-H-060, 30 wt.% PTFE). Experiment was conducted with the flow conditions: $0.5 \times 10^{-4} \leqslant U_L \leqslant 1.0 \times 10^{-3}$ m/s and $0.55 \leqslant U_G \leqslant 9.36$ m/s , and under room temperature (25 °C) and back pressure (1 atm). The range of the liquid and air flow rates is chosen by using the operation condition of PEM fuel cells as reference; and it covers the typical patterns of two-phase flow encountered, i.e. slug, mixed flow, and annulus. Detailed experimental procedure was documented in our previous paper [20]. In the experiment, the channel surface was characterized using optical visualization, including both droplet morphology and rough surface 3-D scan. Two-phase flow pattern and location were recorded through top and cross-sectional visualization, respectively. Real-time two-phase pressure was measured using a pressure transducer.

2.2. Surface characterization

Fig. 2 presents the droplet shapes on the three surfaces and also displays the rough surface of the selected carbon paper. The

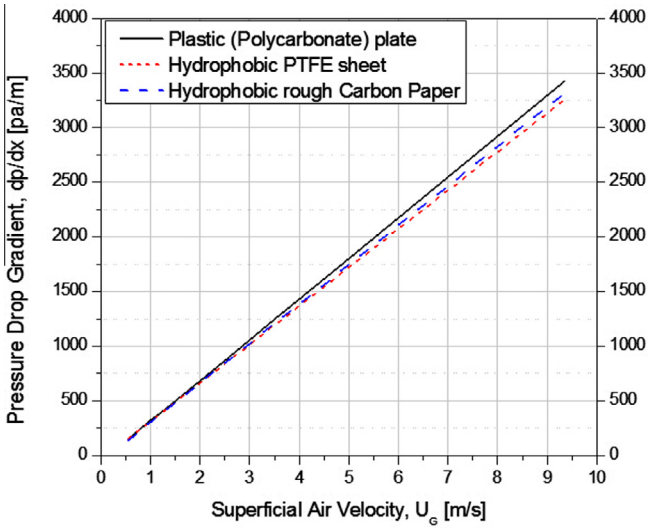

Fig. 3. Single-phase pressure drops in a flow channel under various surface conditions.

contact angle was then measured through the droplet shape. Digital microscope (VHX-600, 54 mega pixels) of KEYENCE was used for the 3-D scan. The 3-D profile measurement unit (VHX-S15CE) was adopted for accurate control of step scanning. As seen from the figure, the three surfaces exhibit different properties: the Polycarbonate surface is hydrophilic ($\theta = 80°$) and smooth (roughness, ~1.3 nm rms [20]). The PTFE sheet is hydrophobic ($\theta = 104°$) with a smooth surface (roughness, 550–226 nm rms [21]). The carbon paper is hydrophobic ($\theta = 128°$) when treated with PTFE. Different with the PTFE sheet, the carbon paper is relatively rough (with a

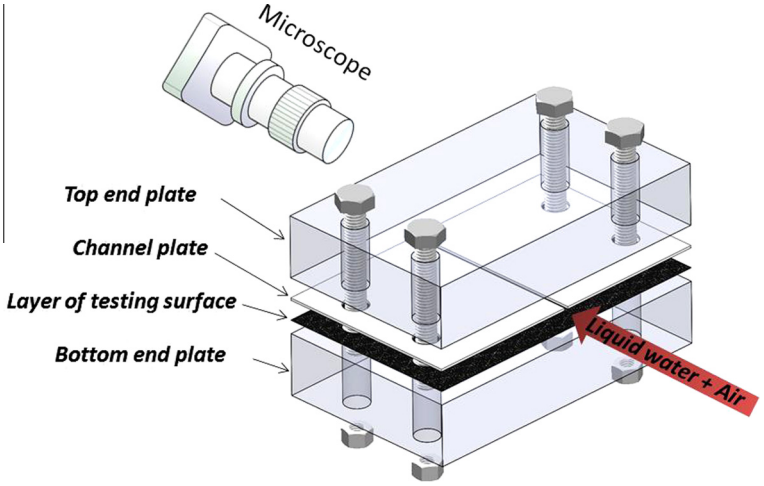

Fig. 4. Schematic of the test section for cross-sectional visualization of two-phase flow.

Table 2
Two-phase pressure correlations and two-fluid model.

Type	Authors	Correlation	Channel dimensions & working fluids
Martinelli-parameter-based model $\left(\frac{dp}{dx}\right)_{TP} = \left(\frac{dp}{dx}\right)_G \Phi_G^2 \Phi_G^2 = 1 + C \cdot X + X^2$ $X^2 = \frac{(dp/dx)_L}{(dp/dx)_G}$	Lockhard and Martinelli [22]	$C = 5$	1.49–25.83 mm Air; water, oil, hydrocarbons
	Mishima and Hibiki [23]	$C_{rec} = 21[1 - \exp(-0.319 D_h)]$ $C_{cir} = 21[1 - \exp(-0.333 D)]$	1.05–4.08 mm Air; water
	Sun and Mishima [24]	$C = 1.79\left(\frac{Re_G}{Re_L}\right)^{0.4}\left(\frac{1-x}{x}\right)^{0.5}$	0.506–12 mm Air; water, refrigerant, CO_2
	Li and Wu [25]	$C = 11.9 Bo^{0.45} \quad (Bo \leqslant 1.5)$ $C = 109.4(Bo Re_L^{0.5})^{-0.56} \quad (1.5 < Bo \leqslant 11)$	0.148–3.25 mm 12 Fluids
	Zhang et al. [26]	$C = 21[1 - \exp(-0.674/Lo^*)]$ (liquid–gas) $C = 21[1 - \exp(-0.142/Lo^*)]$ (liquid–vapor)	0.07–6.25 mm 7 Fluids
	Kim and Mudawar [27]	$C = 3.5 \times 10^{-5} Re_L^{0.44} Su_G^{0.50} \left(\frac{\rho_L}{\rho_G}\right)^{0.48}$	0.0695–6.22 mm 17 Fluids
Two-fluid model [33] $\Delta\bar{P}_G = \bar{x}^* + \int_{x^*}^1 \frac{1}{k_{rG}} d\hat{x}$	Wang [28]	$k_{rL} = s_e^{n_k}$, $k_{rG} = (1 - s_e)^{n_k}$	1.0 mm Air; water (theoretical)
	Nowamooz et al. [29]	$k_{rL} = s_e^{1.15}$, $k_{rG} = (1 - s_e)^{3.05}$	0.429 mm (fracture) Air; water
	Corey [30]	$k_{rL} = s_e^4$, $k_{rG} = (1 - s_e)^2(1 - s_e^2)$	Not specified Gas; oil
	Fourar and Lenormand [31]	$k_{rL} = \frac{s_l^2}{2}(3 - s_l)$, $k_{rG} = (1 - s_l)^3 + \frac{3}{2}\frac{\mu_G}{\mu_L} s_l (1 - s_l)(2 - s_l)$	Viscous coupling model
	Huang et al. [32]	$k_{rL} = \frac{s_l^2}{2}(3 - s_l)$, $k_{rG} = (1 - s_l)\left[\frac{3}{2}\frac{\mu_G}{\mu_L} + (1 - s_l)^2\left(1 - \frac{3}{2}\frac{\mu_G}{\mu_L}\right)\right]$	Analytic modeling based on LBM
	Chen et al. [34]	$k_{rL} = 0.2677 s_l^3 + 0.331 s_l^2 + 0.3835 s_l$ $k_{rG} = 0.502(1 - s_l)^3 + 0.1129(1 - s_l)^2 + 0.3483(1 - s_l)$	0.13 mm (fracture) Air; water

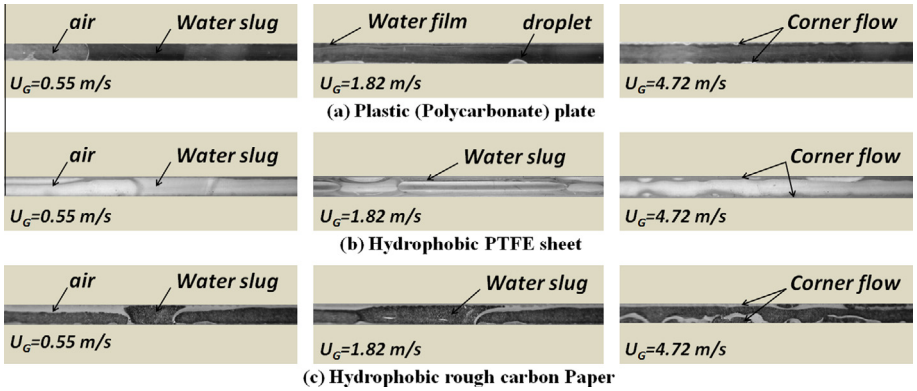

Fig. 5. Two-phase flow pattern visualization for various operating conditions ($U_L = 1.0 \times 10^{-4}$ m/s).

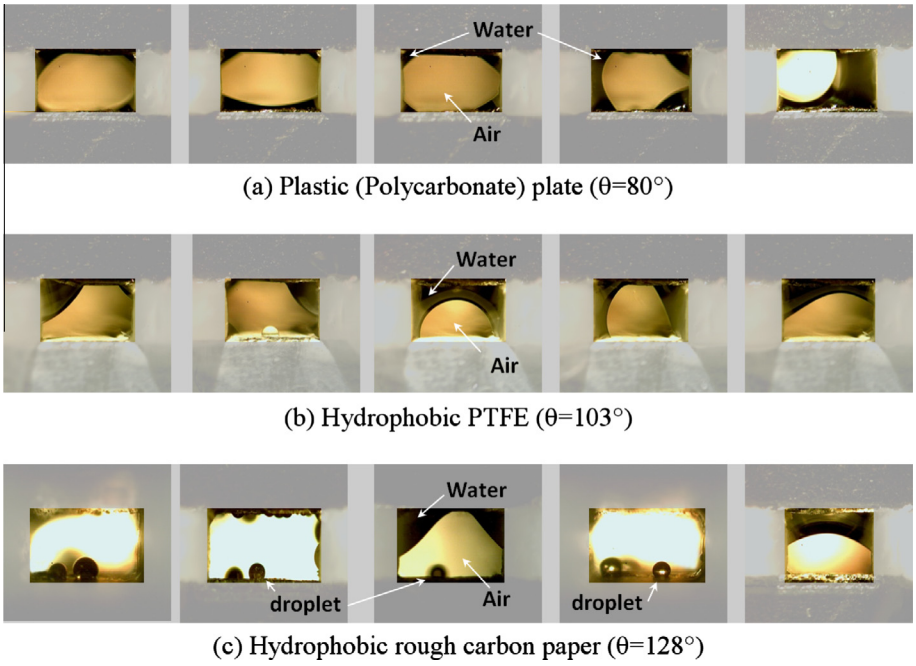

Fig. 6. Cross-sectional visualization of two-phase flow with various bottom surface conditions: (a) hydrophilic Polycarbonate surface, (b) hydrophobic PTFE sheet, and (c) rough carbon paper with 30 wt.% PTFE loading.

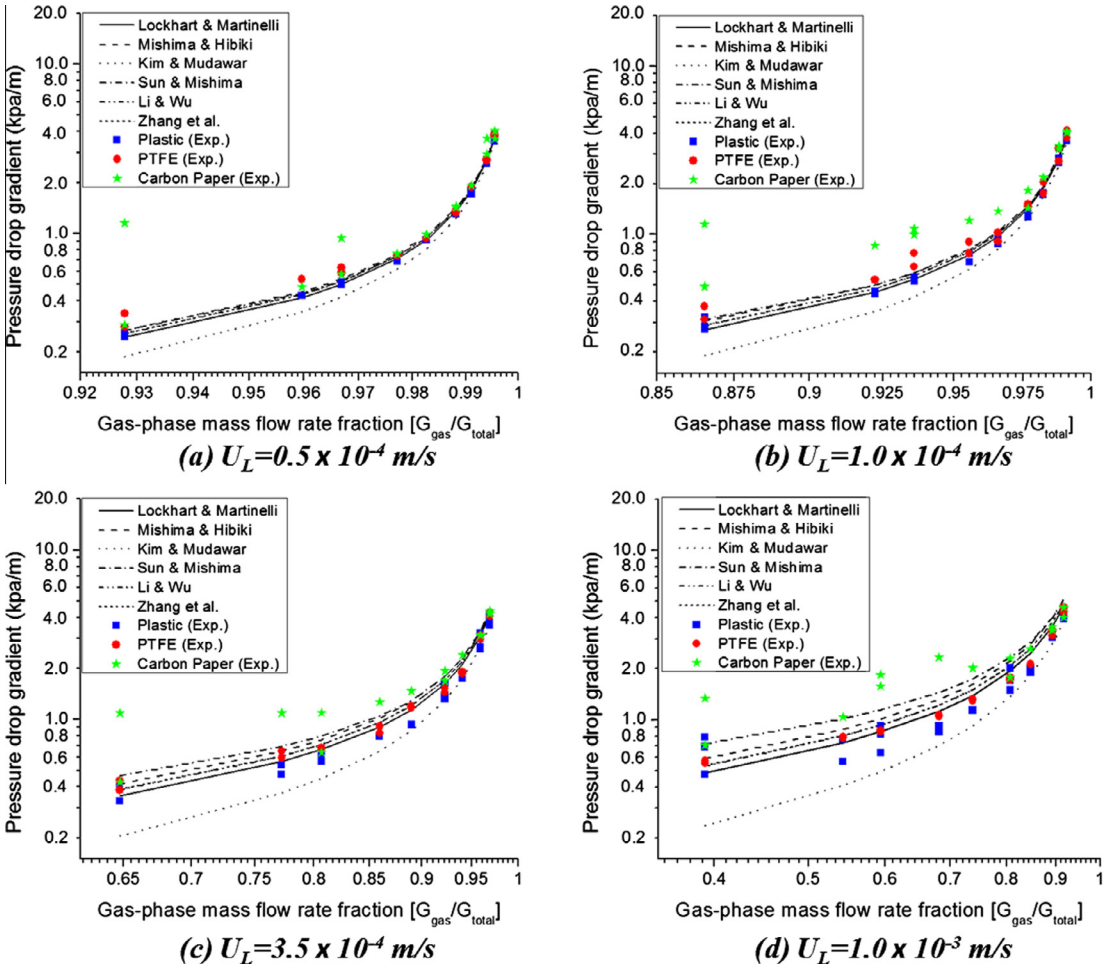

Fig. 7. Two-phase pressure gradients in the channel of the three surfaces, respectively, and comparison with model predictions using the Lockhart–Martinelli parameter.

roughness of 21.5–28.9 μm rms [22]). Table 1 summarizes the three material surfaces and their properties.

2.3. Pressure measurement

Real-time two-phase pressure was measured by a pressure transducer (Setra Model 230) with accuracy of ±0.25% FS. A NI DAQ system (6025E & SCB100) was connected to the pressure transducer to record the data at a frequency of 10 Hz. In addition, the channel cross-sectional area will be altered upon adding a substrate layer between the channel and base plates directly, as a result of material deformation (intrusion) under compression. Given the micro dimension of the channel, such intrusion can considerably alter pressure drop. To minimize material deformation, additional layer is added only under the land area. Compact pressure was then adjusted to ensure comparable single-phase pressures (without any liquid flow) among the three cases, as shown Fig. 3.

2.4. Flow cross-sectional visualization

In experiment, flow pattern was probed by top-view visualization through a transparent plate. Top view, however, cannot reveal the exact site of two-phase flow on the four channel walls. To examine two-phase flow location, the cross-sectional view (in the direction along the channel) is needed. Another experimental device was fabricated for the cross-sectional view. It has the same cross-sectional dimension ($1.68 \times 1.00\ mm^2$) with a shortened length, see Fig. 4. The experimental design is similar to that for the two-phase pressure measurement, except that water and air are directly supplied through one end of the channel. A camera was placed near the outlet of the channel to record liquid water location inside the channel. When two-phase flow becomes unstable, multiple images were taken.

3. Two-phase flow models

In the first paper of this series [20], two groups of two-phase models are explained: they are the Martinelli-parameter-based models and two-fluid models, see Table 2. In particular, Wang [28] extended the flow description in porous media to micro channels, and derived the following expression for pressure drop:

$$\Delta \bar{P}_G = \bar{x}^* + \int_{\bar{x}^*}^{1} \frac{1}{k_{rG}} d\hat{x} \tag{1}$$

where $k_{rG} = (1 - s_e)^{n_k}$ (2)

k_{rG} is the relative permeability for gas phase. s_e is the effective saturation which takes into account the residual liquid saturation, and n_k is the exponent constant. Note that a larger value of n_k represents a larger impact of liquid presence on gas flow.

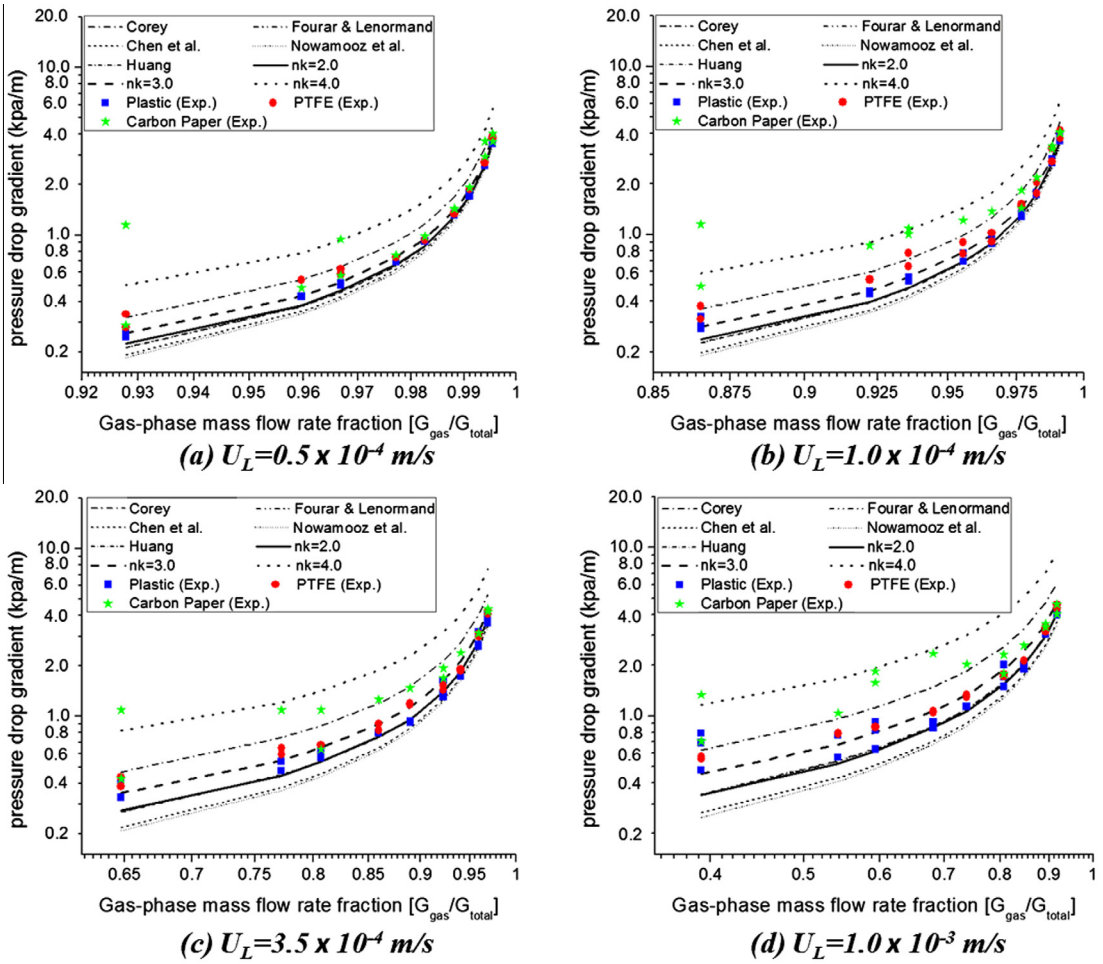

Fig. 8. Two-phase pressure gradients in the channel of the three surfaces, respectively, and comparison with the two-fluid model.

4. Results and discussion

4.1. Two-phase flow pattern

Fig. 5 shows the flow patterns observed for different surfaces. When air superficial velocity is low (U_G = 0.55 m/s) where the inertial force is relatively insignificant, no significant difference is observed among the three surfaces. Under this condition, slug formation occurs. As the air velocity increases to U_G = 1.82 m/s, two-phase flow transits to the mixed pattern of wavy flow and droplet formation for the case with the plastic surface; and slug-like flow is observed for the case with the PTFE sheet and carbon paper. As air velocity further increases to U_G = 4.72 m/s, stable corner flow develops for the plastic surface; wavy corner flow occurs for the cases with the hydrophobic PTFE sheet and carbon paper.

4.2. Cross-sectional visualization

To reveal two-phase location, cross-sectional visualization was taken and images are shown in Fig. 6. For the hydrophilic plastic surface which attracts liquid phase, liquid mostly appears in all the four corners. Thus, the core region of the channel is usually occupied by air flow (unless it is slug flow). In addition, liquid flow may not be evenly distributed among the four corners, particular when the liquid flow rate is high and two-phase flow is unstable. By using

Table 3
Experimentally determined value of n_k (in Eq. (2)) for various flow patterns.

n_k Values	Slug flow	Mixed flow	Annular flow
Plastic	2.49	2.15	1.96
PTFE	2.89	2.58	2.47
Carbon paper	3.76	3.37	2.67

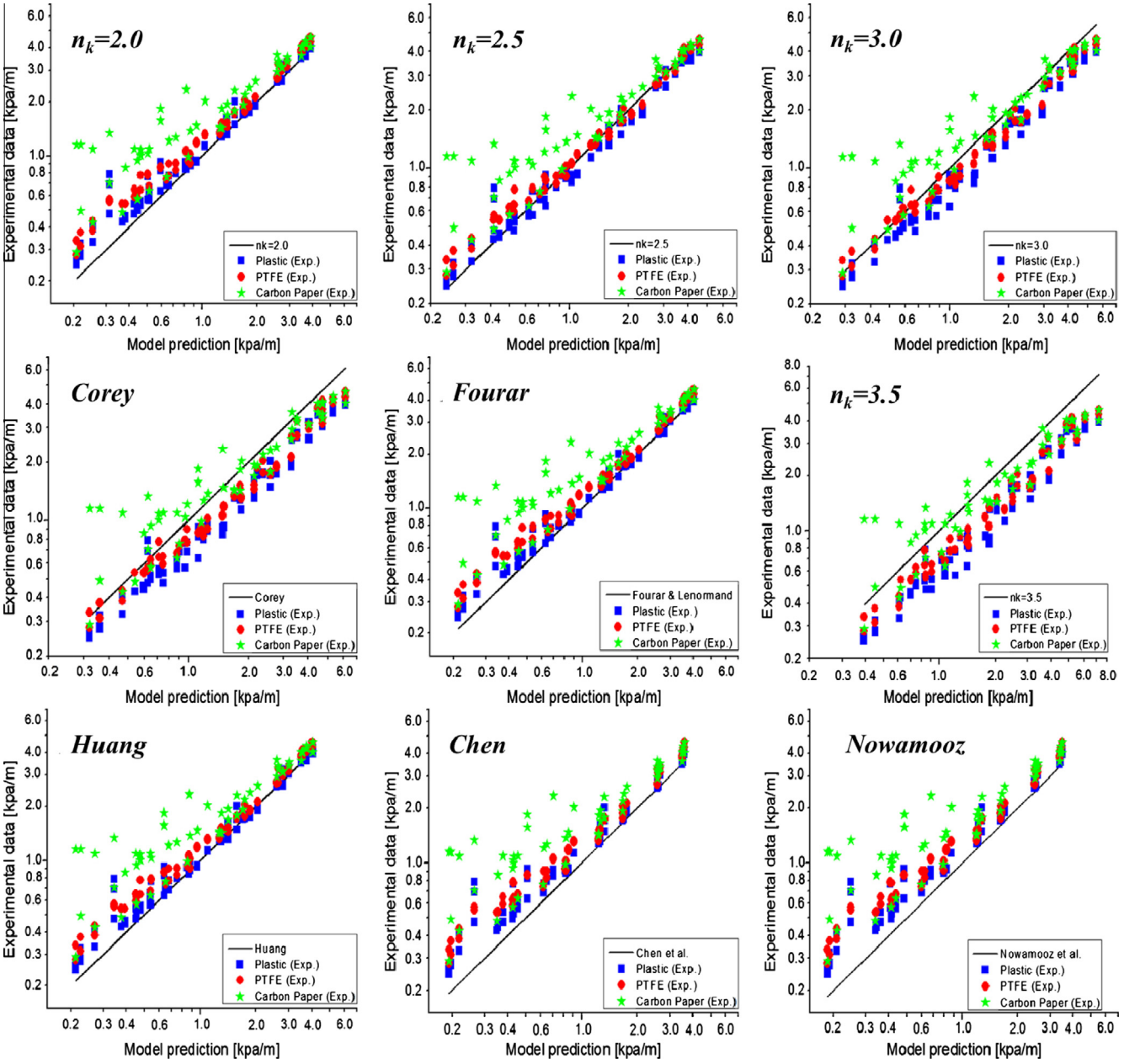

Fig. 9. Comparison of experimental two-phase pressure and various prediction models.

the PTFE sheet which has a hydrophobic smooth surface, the two bottom corners are less likely to be filled with liquid water compared to the plastic surface. Since most water flow is through the two top corners, the corner flow becomes thicker than that in the plastic-surface case under the same flow condition. In addition, the top plate can be all covered by liquid flow though it is not slug yet. However, when observed from the top plate in the previous visualization, the view will show a slug-like pattern. When using the hydrophobic rough carbon-paper surface, liquid water is repelled from the hydrophobic surface to the two top corners. Similar to the PTFE sheet case, slug formation was observed in Fig. 5 for the case of the carbon paper under moderate air velocity; it is clear from Fig. 6 that water slug only covers the top part of the channel; while there is space between the carbon paper and liquid surface for gas flow. Additionally, droplets may attach rough surface; and it can be difficult to remove them on rough surface, as shown in Refs. [35,36]. Droplet presence surely obstructs air flow, increasing pressure drop.

4.3. Two-phase pressure gradient

Figs. 7 and 8 present both experimental data and model prediction. Fig. 7 shows that the empirical model prediction using the Lockhart–Martinelli parameter matches with the experimental data for both the hydrophilic plastic plate and hydrophobic PTFE sheet. For the carbon paper, a portion of the experimental data fall in around the prediction curves; however, some points deviate from the model prediction. More specifically, under low water flow rates, all of the model predictions show acceptable agreement with the experimental data in the regime of high air velocity. As the water flow rate increases, model predictions deviate from the experimental data a little bit, but still within the range. As the air velocity further decreases, experimental data differ among the three surfaces: in particular, the data with the hydrophilic surface still fall around the model prediction. The case with the hydrophobic PTFE sheet surface, in general, shows higher values in the experimental data than those of the hydrophilic plastic surface. This can be explained by the fact that liquid is usually present at the upper two hydrophilic corners thus more liquid accumulation. As to the carbon-paper surface, the measurement is higher than the other two surface conditions. In addition, droplets on the rough surface obstruct gas flow, contributing to the observed larger pressure drop. Fig. 8 presents the two-fluid model predictions using various correlations for the relative permeability. Again, similar trends were observed. Using Eq. (2) for the relative permeability, the prediction curves using $n_k = 2$ and 4 bound most experimental data, including those for the carbon-paper surface.

Fig. 9 presents comparison for each correlation of the relative permeability. Overall, Eq. (2) with $n_k = 2.5$ provides a good prediction for both the hydrophilic and PTFE sheet surfaces. However, in the regime of low pressure (i.e. low air velocity), the curve of using $n_k = 2.5$ shows discrepancy, instead, n_k between 2.5 and 3.0 shows a closer prediction with the experimental data of the plastic surface; while n_k of 3.0 better fits with the data for the hydrophobic PTFE sheet. For the carbon-paper surface, experimental data mostly fall in between the lines of n_k of 3.0 and 4.0.

To obtain a better match with experimental data, the n_k value in Eq. (2) can be further tuned for each flow pattern through minimizing the MAE (Mean Absolute Error). The model predictions using the tuned n_k values are plot in Fig. 10, along with the corresponding MAE values. The values of n_k are listed in Table 3. A higher value of n_k represents a larger impact of liquid flow on gas flow. Based on the analytic solution for annulus flow in a circular channel and 2-D channel, n_k equals to 2.0 and 3.0, respectively [20]. The two values provide the bounds of n_k for the two cases of the hydrophilic plastic surface and smooth PTFE sheet surface. Because liquid is present in all the four walls for the case of the hydrophilic plastic surface, the flow is similar to that analyzed in a circular channel. As a result, the obtained n_k in this case is lower than the other two cases. As to the PTFE sheet, liquid phase preferably flows

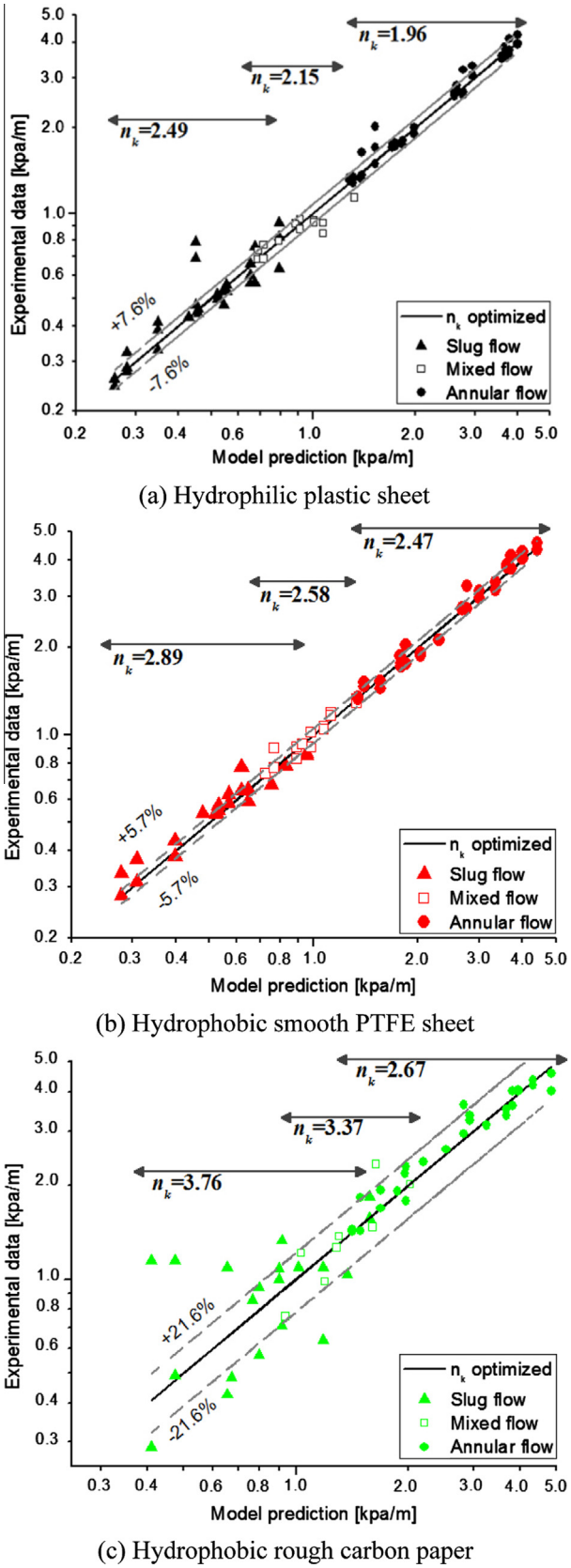

Fig. 10. Determined value of the n_k exponent (in Eq. (2)) for various surfaces and flow patterns.

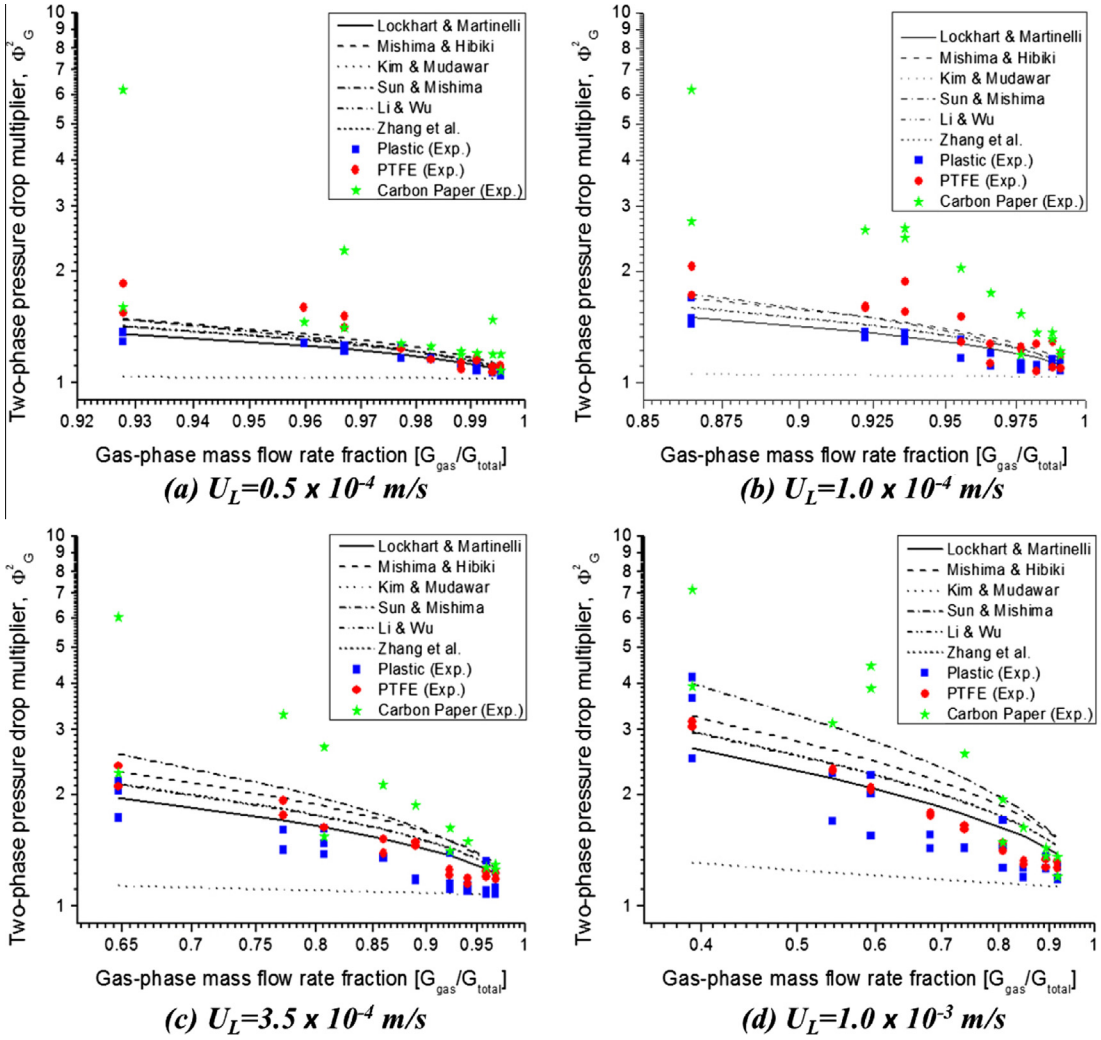

Fig. 11. Two-phase friction multiplier obtained from the experiment and Martinelli-parameter-based models.

on the other three hydrophilic walls, mostly in the upper two corners, making it similar to the flow condition in a 2-D channel. Thus, the value of n_k is close to 3.0. As to the carbon-paper surface, droplets appearing on the rough surface impose obstruction on gas flow, thus n_k is higher. In addition, for hydrophobic carbon papers, n_k of 3.0 or 4.0 has been used in two-phase flow modeling [37,38].

4.4. Two-phase friction multiplier

The experimental two-phase friction multipliers under the three surface conditions are plotted, along with the empirical model prediction, in Fig. 11. Under low water flow rates, the hydrophilic surface and the hydrophobic PTFE sheet are similar, showing a good agreement with the model prediction. As the air velocity decreases or liquid-phase flow rate increases, a larger effect of liquid presence on gas flow (thus higher values of the two-phase friction multiplier) is expected for the PTFE surface. For the carbon-paper surface, the interaction between phases is even higher. As the water flow rate increases, the models show a better match with the measured data at low air velocity and over-predict under high air velocities for the hydrophilic plastic and hydrophobic PTFE surfaces. None of the model prediction follows the trends of measured data for the case of the hydrophobic carbon paper. Fig. 12 presents the measured friction multipliers, along with the two-fluid model prediction. Similarly, no single correlation can be universally applied. This graph also presents the predictions with the tuned n_k values in Eq. (2), which show a good match for each surface condition.

4.5. Real-time two-phase pressure

Fig. 13 shows the real-time pressure for each case under various operating conditions. Pressure spikes are observed for low air velocity cases due to periodic slug formation. Figs. 5 and 6 show that it is difficult for slug to completely block the channel in the two cases with a hydrophobic surface because the non-wetting surface repels liquid. However, bulky liquid may be present in the channel, which attaches all the walls except the hydrophobic surface. Different with the hydrophilic surface, slugs form in a much less frequency in the case with the PTFE sheet: this is likely due to the fact that in the case with the hydrophilic surface liquid water can accumulate in the four channel corners, thus it is prone to slug formation. Additionally for the PTFE sheet, slug formation is not as periodic as that in the hydrophilic surface. This may be due to the hydrophobic surface which prevents liquid from totally blocking the channel, thus bulky liquid can be avoided in some occasions. As to the rough carbon-paper surface, slug formation only appears in $U_L = 1.0 \times 10^{-3}$ m/s and the lowest air flow rate. This may be due to the fact that the rough carbon-paper surface

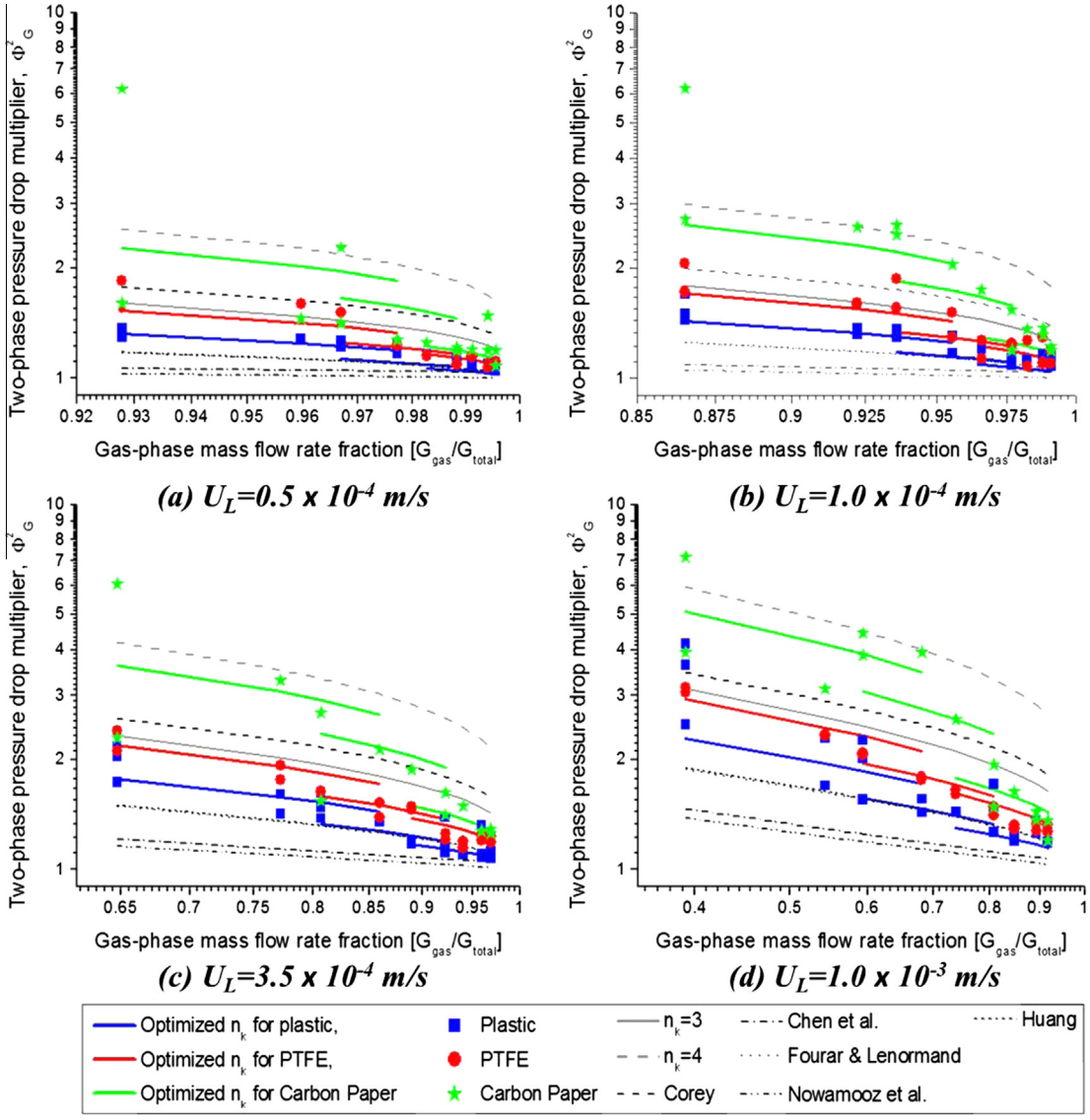

Fig. 12. Two-phase friction multiplier predicted by the two-fluid model.

more likely prevents liquid presence at the two corners consisting of the hydrophobic and hydrophilic surfaces, thus reducing liquid accumulation in the channel space, as opposed to the smooth PTFE sheet. Under higher liquid flow rates, bulky droplets more likely hold on the rough surface, causing local liquid accumulation and slug formation. The frequency of slug formation may be related to droplet formation and formation sites that in general randomly occur. The figure also shows there appear some spikes occurring in short duration for the case with carbon paper. This may be caused by droplet formation and removal: droplets can form on the rough hydrophobic surface, leading to a sudden increase in pressure drop; and their removal can occur in a short period: some detached droplets roll over the rough surface, dragged by air flow; as a result, the pressure drop rapidly decreases, leading to a spike occurring in a short time, as observed.

5. Conclusion

Two-phase flows in a rectangular micro channel with differing surface conditions (wetting property and roughness) were experimentally and numerically investigated. Imaging was conducted to evaluate the surface properties, including contact angle and roughness, and visualize two-phase flow pattern and liquid location in channels through top and cross-sectional views, respectively. The contact angle of the surface ranges from 80° to 124°; and the rough surface has a roughness of 21.5–28.9 μm rms, in comparison with those of smooth surfaces (roughness: 226–550 and ~1.3 nm rms, respectively). We found that in the hydrophilic channel liquid water appears in all the four corners; while when one hydrophilic wall changes to a hydrophobic one, liquid is preferentially presented in the two hydrophilic corners. It was observed that a rough carbon-paper surface makes it difficult to remove droplets attaching the surface. Both empirical models and two-fluid model were employed to predict two-phase flow, showing acceptable agreement with experimental data for the hydrophilic channel and the channel with a smooth PTFE sheet (hydrophobic) surface. For the channel with a hydrophobic rough carbon-paper surface, it was experimentally observed that the pressure oscillates in a wide range under the same condition, which is likely caused by droplet presence on the rough surface. A set of exponent values for the two-fluid model were determined for each flow pattern and the three surfaces, showing surface heterogeneity affects the relative permeability. The rough hydrophobic surface shows the exponent

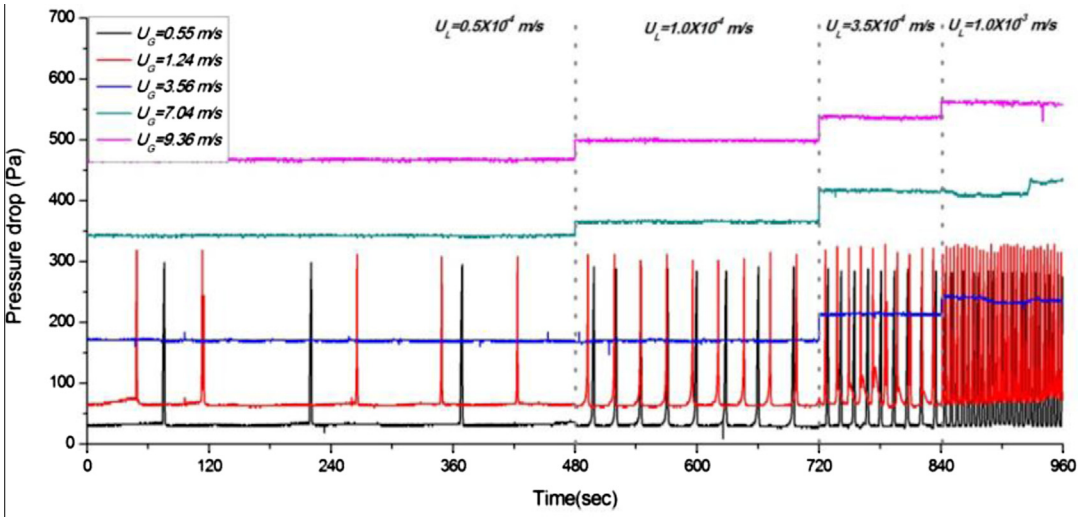

(a) Plastic (Polycarbonate) plate

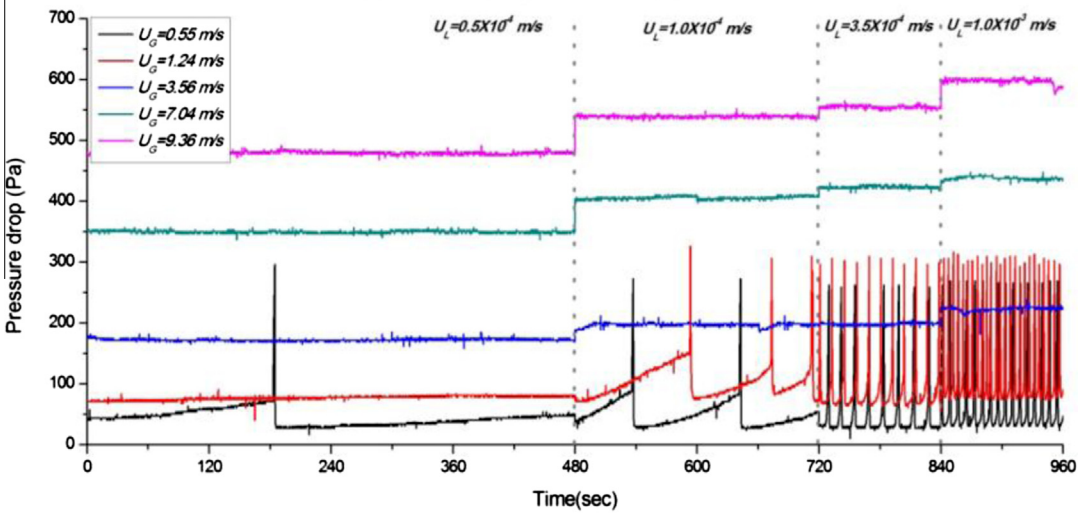

(b) Hydrophobic PTFE sheet

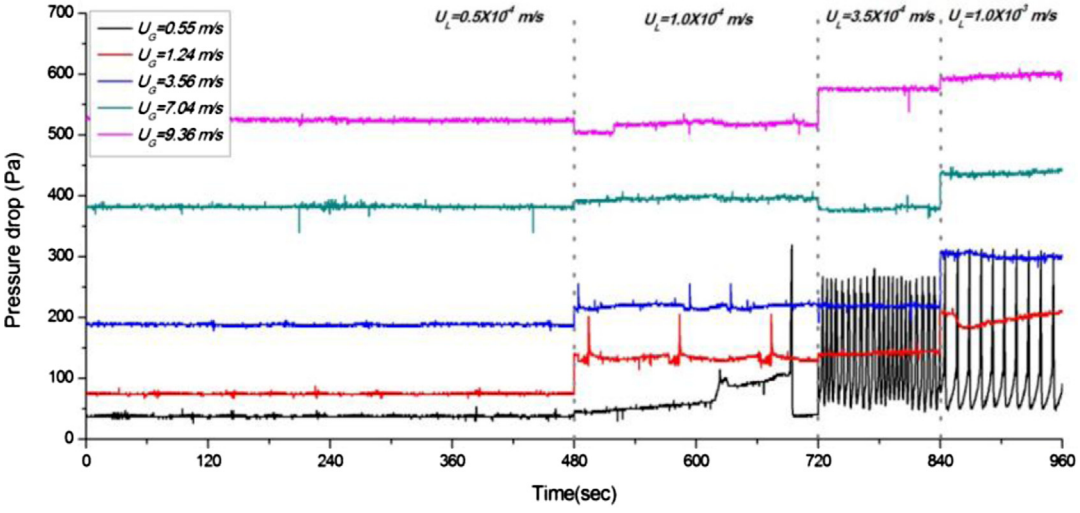

(c) Hydrophobic rough carbon paper (30 wt.% PTFE loading)

Fig. 13. Real-time pressure drop under various surface and operating conditions.

in the power expression of the relative permeability is 2.67 (Annulus regime), 3.37 (Mixed flow regime), and 3.76 (Slug regime), respectively; while the smooth hydrophobic/hydrophilic surface exhibits a value of 2.47/1.96, 2.58/2.15, and 2.89/2.49, respectively. The range of values is consistent with the theoretical analytical results in our previous work and the data used in the literature.

In the real-time pressure data, it was observed that slug formation is more frequent in the purely hydrophilic channel than those with a hydrophobic wall. In the channel with a rough hydrophobic surface, less liquid accumulates in the channel corners, reducing the occurrence of slug flow. In some regimes, droplets attach on the rough surface; and are then removed by air flow, causing pressure spikes.

References

[1] M. Kaji, T. Sawai, Y. Kagi, T. Ueda, Heat transfer and fluid dynamics of air–water two-phase flow in micro-channels, Exp. Therm. Fluid Sci. 34 (4) (2010) 446–453.

[2] G. Hetsroni, A. Mosyak, Z. Segal, E. Pogrebnyak, Two-phase flow patterns in parallel micro-channels, Int. J. Multiphase Flow 29 (3) (2003) 341–360.

[3] S. Saisorn, S. Wongwises, Flow pattern, void fraction and pressure drop of two-phase air–water flow in a horizontal circular micro-channel, Exp. Therm. Fluid Sci. 32 (3) (2008) 748–760.

[4] T. Cubaud, U. Ulmanella, C.M. Ho, Two-phase flow in microchannels with surface modifications, Fluid Dyn. Res. 38 (2006) 772–786.

[5] C. Choi, D.I. Yu, M. Kim, Surface wettability effect on flow pattern and pressure drop in adiabatic two-phase flows in rectangular microchannels with T-junction mixer, Exp. Therm. Fluid Sci. 35 (6) (2011) 1086–1096.

[6] T. Takamasa, T. Hazuku, T. Hibiki, Experimental study of gas–liquid two-phase flow affected by wall surface wettability, Int. J. Heat Fluid Flow 29 (6) (2008) 1593–1602.

[7] C.Y. Lee, S.Y. Lee, Influence of surface wettability on transition of two-phase flow pattern in round mini-channels, Int. J. Multiphase Flow 34 (7) (2008) 706–711.

[8] H.T. Phan, N. Caney, P. Marty, S. Colasson, J. Gavillet, Flow boiling of water in a minichannel: the effects of surface wettability on two-phase pressure drop, Appl. Therm. Eng. 31 (11–12) (2011) 1894–1905.

[9] C.Y. Lee, S.Y. Lee, Pressure drop of two-phase plug flow in round mini-channels: influence of surface wettability, Exp. Therm. Fluid Sci. 32 (8) (2008) 1716–1722.

[10] J.B. Taylor, A.L. Carrano, S.G. Kandlikar, Characterization of the effect of surface roughness and texture on fluid flow-past, present and future, Int. J. Therm. Sci. 45 (10) (2006) 962–968.

[11] H.Y. Wu, P. Cheng, An experimental study of convective heat transfer in silicon microchannels with different surface conditions, Int. J. Heat Mass Trans. 46 (2003) 2547–2556.

[12] A. Olekhnovitch, A. Teyssedou, P. Tye, R. Felisari, An empirical correlation for calculating steam-water two-phase pressure drop in uniformly heated vertical round tubes, Int. J. Multiphase Flow 31 (2005) 358–370.

[13] A. Cavallini, D. Del Col, M. Matkovic, L. Rossetto, frictional pressure drop during vapour–liquid flow in minichannels: modelling and experimental evaluation, Int. J. Heat Fluid Flow 30 (2009) 131–139.

[14] B. Suman, P. Kumar, An analytical model for fluid flow and heat transfer in a micro-heat pipe of polygonal shape, Int. J. Heat Mass Transfer 48 (21–22) (2005) 4498–4509.

[15] G.P. Peterson, H.B. Ma, The theoretical analysis of the maximum heat transport in triangular grooves – a study of idealized micro heat pipes, J. Heat Transfer 118 (3) (1996) 731.

[16] S.C. Wong, Y.C. Lin, Effect of copper surface wettability on the evaporation performance: tests in a flat-plate heat pipe with visualization, Int. J. Heat Mass Transfer 54 (17–18) (2011) 3921–3926.

[17] J. Qu, H. Wu, P. Cheng, Effects of functional surface on performance of a micro heat pipe, Int. J. Heat Mass Transfer 35 (5) (2008) 523–528.

[18] H.Y. Wu, P. Cheng, An experimental study of convective heat transfer in silicon micro-channels with different surface conditions, Int. J. Heat Mass Transfer 46 (2003) 2547–2556.

[19] S.S. Hsieh, C.Y. Lin, Convective heat transfer in liquid mocrochannels with hydrophobic and hydrophilic surface, Int. J. Heat Mass Transfer 52 (1–2) (2009) 260–270.

[20] S.C. Cho, Y. Wang, Two-phase flow dynamics in a micro hydrophilic channel: a theoretical and experimental study, Int. J. Heat Mass Transfer 70 (2014) 340–352.

[21] M.C. Zhang, E.T. Kang, K.G. Neoh, K.L. Tan, Surface modification of aluminum foil and PTFE film by graft polymerization for adhesion enhancement, Collids Surf. A: Physicochem. Eng. Aspects 176 (2–3) (2001) 139–150.

[22] C. Leising, Fuel Cell Gas Diffusion Layer Inspection with 3D Profilometry, Nanovea Application Notes, 2010.

[23] K. Mishima, T. Hibiki, Some characteristics of air-water two-phase flow in small diameter vertical tubes, Int. J. Multiphase Flow 22 (1996) 703–712.

[24] L. Sun, K. Mishima, Evaluation analysis of prediction methods for *two-phase flow* pressure drop in mini-channels, Int. J. Multiphase Flow 35 (2009) 47–54.

[25] W. Li, Z. Wu, A general correlation for adiabatic two-phase pressure drop in micro/mini-channels, Int. J. Heat Mass Transfer 53 (2010) 2732–2739.

[26] W. Zhang, T. Hibiki, K. Mishima, Correlations of two-phase frictional pressure drop and void fraction in mini-channel, Int. J. Heat Mass Transfer 53 (2010) 453–465.

[27] S.M. Kim, I. Mudawar, Universal approach to predicting two-phase frictional pressure drop for adiabatic and condensing mini/micro-channel flows, Int. J. Heat Mass Transfer 55 (2012) 3246–3261.

[28] Y. Wang, Porous-media flow fields for polymer electrolyte fuel cells. II: Analysis of channel two-phase flow, J. Electrochem. Soc. 156 (10) (2009) B1134–B1141.

[29] A. Nowamooz, G. Radilla, M. Fourar, Non-Darcian two-phase flow in a transparent replica of a rough-walled rock fracture, Water Resour. Res. 45 (2009) W07406.

[30] A.T. Corey, The interrelation between gas and oil relative permeabilities, Producers Mon. 19 (1954) 38.

[31] M. Fourar, R. Lenormand, A viscous coupling model for relative permeabilities in fractures, Paper SPE 49006 presented at the SPE Annual Technical Conference and Exhibition, New Orleans, LA, 1998.

[32] H. Huang, Z. Li, S. Liu, X.Y. Lu, Shan-and-Chen-type multiphase lattice Boltzmann study of viscous coupling effects for two-phase flow in porous media, Int. J. Numer. Methods Fluids 61 (2009) 341–354.

[33] X.C. Adroher, Y. Wang, Ex-situ and modeling study of two-phase flow in a single channel of polymer electrolyte membrane fuel cells, J. Power Sour. 196 (2011) 9544–9551.

[34] C.Y. Chen, R.N. Horne, M. Fourar, Experimental study of liquid–gas flow structure effects on relative permeabilities in a fracture, Water Resour. Res. 40 (8) (2004) W08301.

[35] S.C. Cho, Y. Wang, K.S. Chen, Droplet dynamics in a polymer electrolyte fuel cell gas flow channel: forces, deformation and detachment. II: Comparisons of analytical solution with numerical and experimental results, J. Power Sour. 210 (2012) 191–197.

[36] S.C. Cho, Y. Wang, K.S. Chen, Droplet dynamics in a polymer electrolyte fuel cell gas flow channel: forces, deformation, and detachment. I: Theoretical and numerical analyses, J. Power Sour. 206 (2012) 119–128.

[37] Y. Wang, C.Y. Wang, A non-isothermal, two-phase model for polymer electrolyte fuel cells, J. Electrochem. Soc. 153 (2006) A1193.

[38] Y. Wang, C.Y. Wang, Two-phase transients of polymer electrolyte fuel cells, J. Electrochem. Soc. 154 (2007) B636.